China Geology 7 (2024) 315−329

China Geology

Journal homepage: http://chinageology.cgs.cn
https://www.sciencedirect.com/journal/china-geology

Automated machine learning for rainfall-induced landslide hazard mapping in Luhe County of Guangdong Province, China

Tao Li[a, b], Chen-chen Xie[a, b, c], Chong Xu[a, b,*], Wen-wen Qi[a, b], Yuan-dong Huang[a, b, d], Lei Li[a, b]

[a] *National Institute of Natural Hazards*, *Ministry of Emergency Management of China*, *Beijing* 100085, *China*
[b] *Key Laboratory of Compound and Chained Natural Hazards Dynamics*, *Ministry of Emergency Management of China*, *Beijing* 100085, *China*
[c] *Institute of Disaster Prevention*, *Sanhe* 065201, *China*
[d] *School of Emergency Management Science and Engineering*, *University of Chinese Academy of Sciences*, *Beijing* 100049, *China*

ARTICLE INFO

Article history:
Received 4 July 2023
Received in revised form 24 August 2023
Accepted 11 March 2024
Available online 25 April 2024

Keywords:
Landslide hazard
Heavy rainfall
Harzard mapping
Hazard assessment
Automated machine learning
Shallow landslide
Visual interpretation
Luhe County
Geological hazards survey engineering

ABSTRACT

Landslide hazard mapping is essential for regional landslide hazard management. The main objective of this study is to construct a rainfall-induced landslide hazard map of Luhe County, China based on an automated machine learning framework (AutoGluon). A total of 2241 landslides were identified from satellite images before and after the rainfall event, and 10 impact factors including elevation, slope, aspect, normalized difference vegetation index (NDVI), topographic wetness index (TWI), lithology, land cover, distance to roads, distance to rivers, and rainfall were selected as indicators. The WeightedEnsemble model, which is an ensemble of 13 basic machine learning models weighted together, was used to output the landslide hazard assessment results. The results indicate that landslides mainly occurred in the central part of the study area, especially in Hetian and Shanghu. Totally 102.44 s were spent to train all the models, and the ensemble model WeightedEnsemble has an Area Under the Curve (AUC) value of 92.36% in the test set. In addition, 14.95% of the study area was determined to be at very high hazard, with a landslide density of 12.02 per square kilometer. This study serves as a significant reference for the prevention and mitigation of geological hazards and land use planning in Luhe County.

1. Introduction

In China, landslides are a common geological hazard that causes catastrophic damage to residents' lives and property (Haque U et al., 2019; Huang YD et al., 2022). According to the China Natural Resources Bulletin, 3668 geological disasters occurred in China in 2023, including 925 landslides that have caused destructive casualties and economic losses. Landslide hazard assessment is pervasively considered as a significant method for enhancing landslide risk management ability. In recent decades, many scholars have applied various methods for landslide hazard assessment (Cui YL et al., 2023; Guo ZZ et al., 2023; Ma SY et al., 2023a), which can be broadly distinguished into two categories, namely, qualitative and quantitative methods. Specifically, qualitative methods primarily rely on expert experience combined with relevant geoscience theories. While qualitative methods are characterized by their simplicity and convenience in application (Abella EAC and Van Westen CJ, 2008; Panchal S and Shrivastava AK, 2022), they mainly rely on subjective judgments from experts. This may inevitably lead to some subjective errors that can influence the accuracy of the assessment results. By comparison, quantitative methods are approaches based on physical processes or data-driven techniques. The physical-based models predict landslides by analyzing the mechanism of landslide occurrence (Ma SY et al., 2022, 2023b, 2023c). Currently, physical-based models commonly used for landslide hazard assessment include SHALSTAB (Montgomery DR et al., 1997), SINMAP (Nery TD and Vieira BC, 2015), and TRIGRS(Baum RL et al., 2010; Ma SY et al., 2022). While these models are able to simulate the physical mechanism of landslide occurrence and are considered effective methods for landslide hazard analysis (Fell R et al., 2008), they require a huge number of rock mass parameters as model inputs. Obtaining these parameters is often challenging, thereby limiting their application in large-

First author: *E-mail address*: litaomail@163.com (Tao Li).

* Corresponding author: *E-mail address*: xc11111111@126.com (Chong Xu).

Literary editor: Xi-jie Chen
doi:10.31035/cg2024064
2096-5192/© 2024 China Geology Editorial Office.

scale regions. The data-driven models evaluate areas where future landslides are likely to occur by measuring the combination of factors that induced landslides in the past, such as logistic regression (Cui YL et al., 2021), information value (Wen BY et al., 2020), frequency ratio (Hong HY et al., 2015), support vector machine (Ma SY and Xu C, 2019), decision tree (DT) (Ali MZ et al., 2021), random forest (RF) (Dou J et al., 2019). These models operate under the premise that landslides occur in areas with similar topographic and geological conditions. In comparison, quantitative methods reduce the interference of subjective factors by establishing mathematical relationships between variables, and often show higher accuracy than qualitative ones (Ko Ko C et al., 2004; Singh K and Kumar V, 2018). However, simply considering quantitative methods as a replacement for qualitative methods is inaccurate, and a more reasonable perspective is that they complement each other (Wang P et al., 2018; Zhang WG et al., 2022).

With the rapid development of artificial intelligence, machine learning has become increasingly popular in addressing nonlinear relationship problems, especially ensemble learning models. For landslide susceptibility analysis, numerous researchers have used different ensemble learning techniques such as bagging, boosting, and stacking algorithms, achieving fruitful and satisfactory results. For instance, Zhang TY et al. (2022) utilized the bagging method in combination with DT, logistic model tree (LMT), and reduced error pruning tree (REPT) and successfully established three bag-hybrid tree-based models: Bag-DT, Bag-LMT, and Bag-REPT for landslide susceptibility assessment in Chenggu County, China. Their results showed that the highest accuracy value (92.5%) was obtained by the Bag-REPT model. Based on two ensemble learning models, RF and extreme gradient boosting (XGBoost), Zhang WG et al. (2023) conducted landslide susceptibility mapping in Fengjie County, China. The AUC values are 0.866 (RF) and 0.864 (XGBoost), respectively, demonstrating that both models achieved accurate results. By comparing the performance of four ensemble models, namely, gradient boosting machine (GBM), categorical boosting (CatBoost), XGBoost, and light gradient boosting machine (LightGBM) in landslide susceptibility assessment in Turkey, Sahin EK (2022) found that the CatBoost model exhibits the best predictive ability , with an AUC value of 0.8975.

As mentioned above, these machine learning methods can learn and discover hidden and unknown patterns in databases (Tsangaratos P and Ilia I, 2016) with high precision. However, as machine learning models become more complex in structure and deeper in technology, it becomes increasingly difficult for researchers to use the techniques in mathematical modeling. Automated machine learning frameworks are well-placed to alleviate the difficulties that researchers may face in using machine learning. These frameworks broaden the application range of machine learning models, mainly by reducing excessive interaction with the users. As one of the automated machine learning frameworks, AutoGluon can combine the strengths of multiple basic machine learning models by training and weighting them together to obtain better output. This platform does not require much user interaction through automatic hyperparameter optimization and algorithm selection, which is very friendly to users who lack programming expertise. In terms of landslide hazard analysis, Qi WW et al. (2021) introduced the AutoGluon framework into landslide hazard assessment for the first time. They conducted a systematic hazard assessment of landslides triggered by the 2017 Jiuzhaigou earthquake based on AutoGluon. The results showed that the total time spent for data preprocessing and training of 11 machine learning models embedded in the AutoGluon is 47.33 s, and the highest AUC value in the test set is 0.94. This experiment shows that AutoGluon can largely improve the efficiency and accuracy of landslide hazard analysis simultaneously.

In this study, 14 machine learning models embedded in the AutoGluon were used to conduct the hazard assessment of rainfall-induced landslides in Luhe County, Guangdong Province. By training 13 basic machine learning models and weighting their outputs, a landslide hazard assessment model was obtained. The main purpose of this study is to provide a scientific basis or reference for the prevention and management of rainfall-induced landslides in Luhe County.

2. Data methods

2.1. Study area

Luhe County is situated in the eastern part of Guangdong Province, China (Fig. 1), with the Tropic of Cancer crossing the county. This county has a total area of 986 km^2 (from 115°24'E, 23°6'N to 115°49'E, 23°28'N). Luhe County falls within the subtropical monsoon climate zone, characterized by a mild climate, with an average annual temperature of approximately 21.5°C. The region receives abundant rainfall mainly concentrated in the summer and autumn, with an average annual precipitation reaching 2324 mm. Topographically, Luhe County is located on the southeast side of the Lianhua Mountains, with the overall relief being high in the east and west and low in the center. The central and southern parts are river terraces and alluvial plains, with an elevation ranging from 5–1173 m. In addition, local faults are mainly concentrated in the northeast direction, and the outcrops are mainly Jurassic and Quaternary granite.

2.2. Data

2.2.1. Landslide inventory

A complete and accurate landslide inventory is a prerequisite for landslide assessment (Fan W et al., 2017). Based on the landslide inventory, the statistical relationship between landslides and relevant influencing factors can be analyzed and used for future landslide prediction (Van Westen CJ et al., 2006; Xu C et al., 2014). Since August 27 to 31, 2018, Luhe County has been constantly hit by heavy rainfall with an average daily precipitation of 70.28 mm,

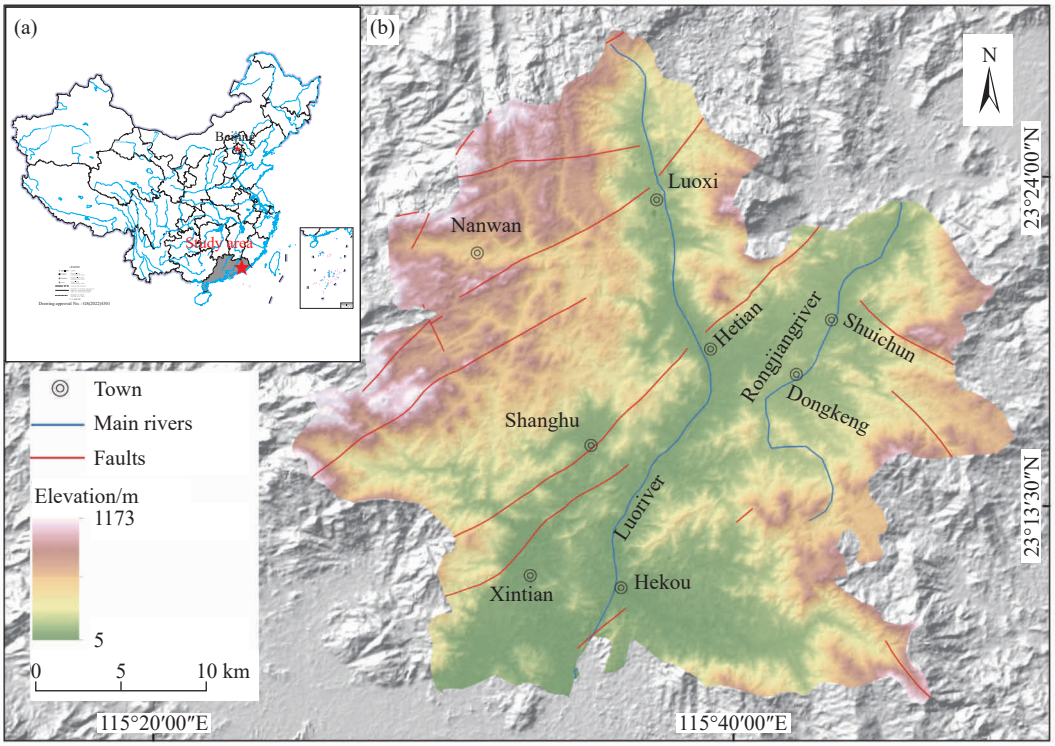

Fig. 1. Location of the study area. a–Location of b, the pentagram marks the location of the study area; b–Topographic map of Luhe County.

which induced a large number of landslides. In this study, planet satellite images with a resolution of 3 m before and after the rainfall were selected as global monthly-scale synthetic images for July and September, 2018, respectively, in order to ensure that the landslides were triggered by this rainfall event. Human-computer visual interpretation was used to identify the landslides, which is more accurate than other automatic identification methods, although the time and cost are higher. Finally, totally 2241 landslides were identified (Fig. 2a), showing that the landslides are mainly distributed in the central part of the study area (Hetian and Shanghu town). The smallest landslide area is 126 m^2, while the largest reaches 19761 m^2. According to the obtained point density map (Fig. 2a), the landslide density reaches a maximum of 54.03/km^2. In about 26% of the landslide abundance areas (Fig. 2b), the number of landslides accounts for 84.29% of the total, with an average landslide density of 7.36/km^2. Fig. 3 shows the comparison between pre- and post-hazard high-resolution satellite images of several landslide abundance areas. Specifically, Fig. 3b and Fig. 3d are located in Hetian Town, Fig. 3f is located in Shanghu Town, and Fig. 3h is located at the junction of Shanghu Town, Hekou Town, and Xintian Town. The images show that the landslides in these four abundance areas are mostly shallow and narrow landslides with long transportation paths. Overall, most of the landslides are distributed on both sides of the valleys, displaying a clear clustered pattern. According to the classification of landslide types by Hungr O et al. (2014), the landslides are mainly debris avalanches. In addition, 2241 non-landslide points were selected as negative samples based on the visual interpretation of satellite images. Together with 2241 landslide points, all data were randomly divided into training set (70%) and test set (30%) for subsequent experiments. In this study, the rainfall-induced landslides that had been well documented by the remotely sensed imagery and investigative data were employed to build the database.

2.2.2. *Causative factors*

The selection of influencing factors is an important step in landslide hazard modeling. However, there is no uniform regulation in the selection of causative factors (Chen W et al., 2018; Abuzied SM and Alrefaee HA, 2019). According to the availability and accuracy of the data, the authors selected 10 causative factors to construct the assessment indicator system by considering four categories of influencing factors: triggering factor, topographical, geological and geomorphological, and anthropogenic factors. The detailed information is shown in Table 1.

As the triggering factor, rainfall alters the water content in the slope body, increase the pore water pressure in the rock-soil mass, and reduce the shear strength, thus is closely related to the landslide occurrence. In this work, rainfall data from rainfall stations under the China Meteorological Administration were collected (Fig. 4a), and the inverse distance weighting (IDW) interpolation method was used to obtain the rainfall data. Fig. 4b presents the daily rainfall data collected for the study area from August 1 to September 9. It is prominent that from August 27 to 31, the lowest daily rainfall is 27.61 mm on August 27 and the highest daily rainfall is 118.45 mm on August 30. The cumulative rainfall steadily increases without significant fluctuations before the rainfall event. However, it rises from 240.41 mm to 564.22 mm during this rainfall event, exhibiting a steep upward trend.

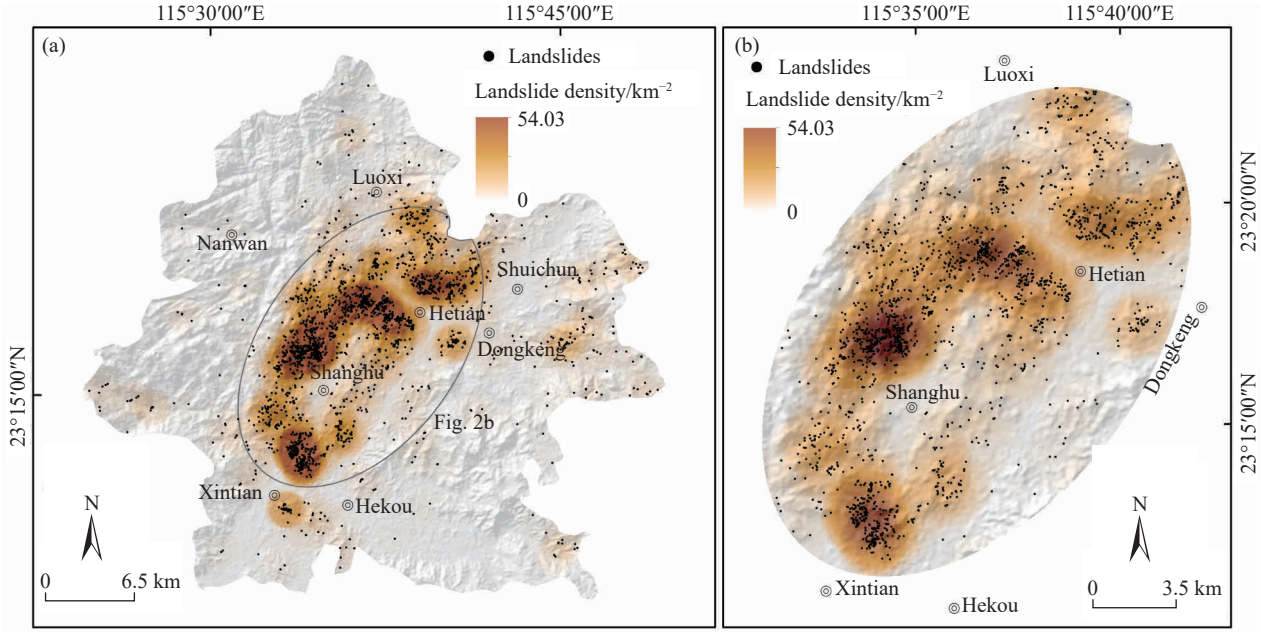

Fig. 2. a–Spatial distribution of landslides and landslide density; b–map showing the zooming of the landslide abundance area.

Five-day cumulative rainfall (Fig. 5a) indicates that the rainfall ranges from 259.86 mm to 403.70 mm.

In terms of topographic-related factors (Fig. 5), elevation is an essential one since different elevations can result in different stress distributions on the slope, which is tightly associated with the stability of the slope. Different aspects can lead to differences in the sunlight received by the slope surface, which can affect regional water evaporation and temperature, resulting in differences in vegetation growth and weathering (Zhang YH et al., 2019). The aspect thematic map was reclassified into nine categories: Flat, north, northeast, east, southeast, south, southwest, west, northwest. Theoretically, the steeper the slope, the more possibility of landslide occurrence. However, some studies have shown that moderate-dipping slopes are more susceptible to landslides (Dai FC and Lee CF, 2002; Cui YL et al., 2022). The TWI typically reflects the moisture condition of the soil under ideal circumstances and has a certain effect on landslide occurrence. In terms of geological and geomorphological factors, different strata possess varying weathering resistance and cohesion, which is one of the critical factors affecting landslide stability. The constant erosion of the river on slope foot weakens the stability of the rock-soil mass on both sides and may eventually causes landslide hazards. NDVI reflects the vegetation cover; higher NDVI values represent higher vegetation coverage in the area, and the root system of plants can strengthen the stability of the slope. The land cover reflects the disturbance caused by human activities to the rock-soil mass, which destroys the stability of the regional ecosystem. Road construction and slope blasting can bring damage to the shear strength of the slope, thereby potentially increasing the risk of geological hazards (Li XS et al., 2022). Therefore, the distance to roads and land cover are factors related to human activities.

To determine the degree of correlation among the impact factors, it should be ensured that none of the independent variables can be linearly represented by other independent variables. Therefore, a Pearson correlation analysis on all factors was conducted. The Pearson correlation coefficient is defined as the quotient of the covariance and standard deviation between two variables (Yao JY et al., 2020), with a coefficient value between −1 and 1. When the value (r) is 0, it indicates that the random variables are linearly independent of each other, while when the absolute value of r is larger, it indicates that the correlation between the random variables is stronger (Eq. 1).

$$r = \frac{\sum_{i=1}^{n}(x_i-\bar{x})(y_i-\bar{y})}{\sqrt{\sum_{i=1}^{n}(x_i-\bar{x})^2}\sqrt{\sum_{i=1}^{n}(y_i-\bar{y})^2}} \quad (1)$$

where n is the number of variables, x_i and y_i are the ith variables x and y, respectively, and $\bar{x}$ and $\bar{y}$ are the average values of x_i and y_i, respectively.

2.3. Method

AutoGluon, an automated machine learning framework developed by Amazon Web Services (AWS), can support automated machine learning for text, image, and tabular data. Focusing on the Tabular module, AutoGluon can train machine learning models on datasets, enabling a highly automated workflow with only a single line of code (Erickson N et al., 2020).

In AutoGluon, there are three key technologies. The first technology is stacking. AutoGluon can train multiple different models on the same data. The outputs of these models are weighted as inputs to a linear model to obtain the final output. The second technology is k-fold bagging that represents the process of dividing the dataset into k non-overlapping data

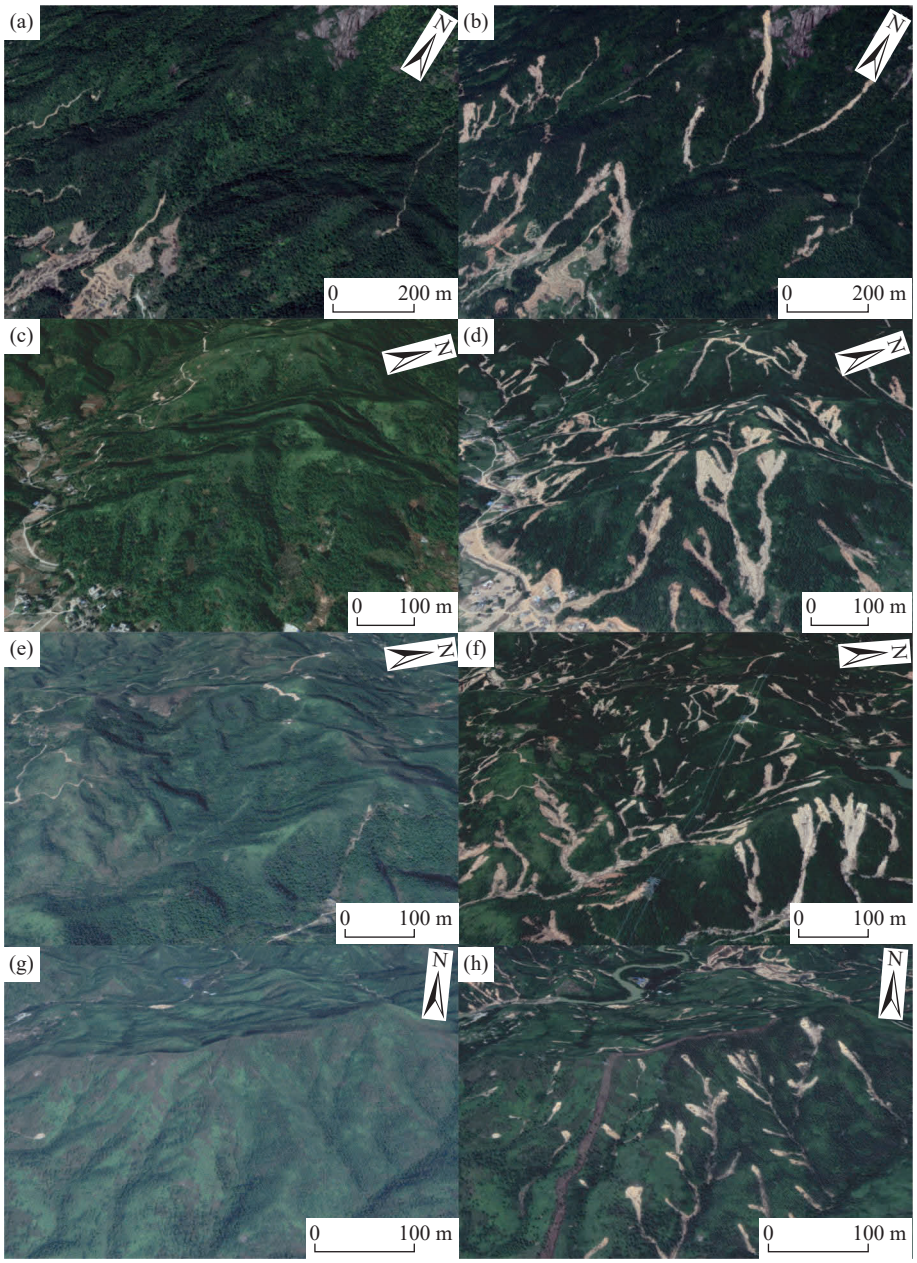

Fig. 3. Examples of images of landslide abundance areas. Landslide distribution before and after the rainfall, and the light colored blocks on the remote sensing map represent the landslides. The coordinates of (a) and (b) are 23°19′38″N, 115°39′12″E; the coordinates of (c) and (d) are 23°18′46″N, 115°36′40″E; the coordinates of (e) and (f) are 23°16′53″N, 115°34′28″E; the coordinates of (g) and (h) are 23°12′21″N, 115°33′59″E.

folds. Each data fold is used in turn as a validation set, while the remaining folds are processed as a training set. The results are then averaged, reducing the variance in the predictions (Parmanto B et al., 1996). The third technology is multi-layer stacking (Erickson N et al., 2020), which is used to combine the output of each model with the data and perform stacking again. This process can be repeated multiple times, and finally a linear model is used as output. As shown in Fig. 6, after the raw data is input and automatically preprocessed, multiple basic machine learning models are trained on the same datasets, and their outputs are concatenated and then fed into the next layer. Unlike the conventional stacking approach, AutoGluon not only takes the output of the previous layer as the input to the stacking layer, but also the features of original data. In the stacking layer, the outputs from the previous layer are combined with the data features as inputs for retraining. The outputs of the final stacking layer are weighted to form the linear model WeightedEnsemble, which combines the strengths of each base machine learning model (Erickson N et al., 2020). AutoGluon adopts a multi-layer stacking strategy for model training. To prevent overfitting during the automated process and improve model performance, k-fold bagging is applied to each machine learning model.

This study utilizes 14 mathematical models embedded in AutoGluon, including KNeighborsDist, KNeighborsUnif, XGBoost, CatBoost, LightGBMLarge, LightGBM, LightGBMXT, RandomForestEntr, RandomForestGini, ExtraTreesEntr, ExtraTreesGini, NeuralNetFastAI,

Table 1. Landslide causative factors and sources.

Factor	Data type	Data source
Elevation	Grid (30 m)	ASTGTM2 DEM (https://www.gscloud.cn)
Slope	Grid (30 m)	From DEM
Aspect	Grid (30 m)	From DEM
NDVI	Grid (250 m)	MODIS MOD13Q1 (https://www.gscloud.cn)
TWI	Grid (30 m)	From DEM
Land cover	Grid (30 m)	GLOBELAND30 (http://www.globallandcover.com)
Lithology	Polygon	1:200000 Geological map (https://www.ngac.cn/)
Distance to roads	Line	National Catalogue Service for Geographic Information (https://www.webmap.cn)
Distance to rivers	Line	From DEM
Rainfall	Point	National Meteorological Information Center (http://data.cma.cn)

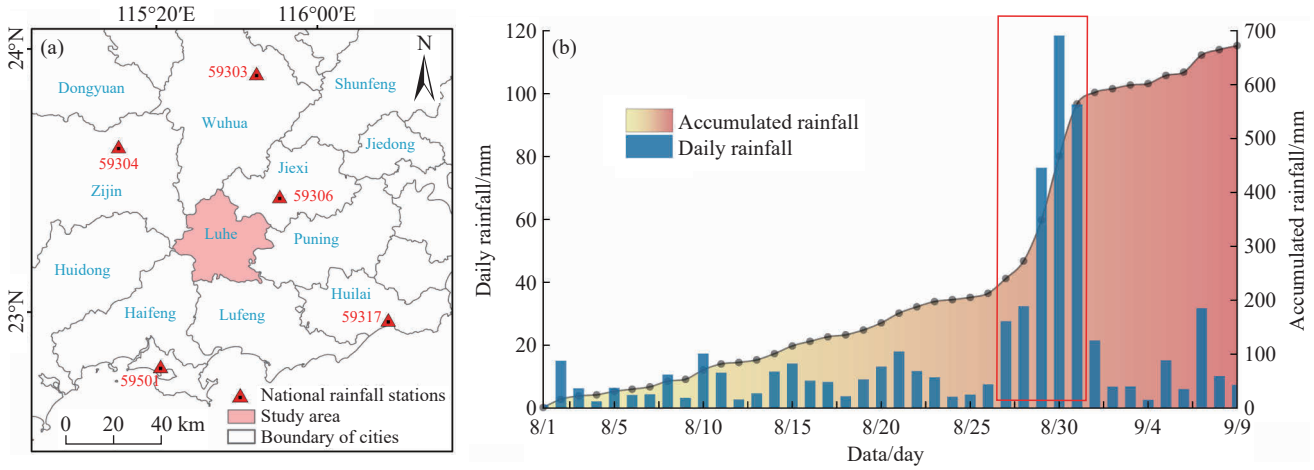

Fig. 4. Rainfall data for the study area. a–distribution of precipitation stations. b–rainfall data from August 1 to September 9, 2018. The red rectangle shows the daily rainfall from August 27 to 31.

NeuralNetTorch, and the final ensemble model WeightedEnsemble. Among them, KNeighborsDist and KNeighborsUnif belong to the same KNeighbors model, while the difference lies in the different choices of weight parameters in the algorithm. XGBoost, CatBoost and LightGBM all belong to the models under the framework of GBDT algorithm. LightGBM is an optimized model on the conventional GBDT algorithm (Ke GL et al., 2017), and there are LightGBMLarge and LightGBMXT with modified parameters in addition to the LightGBM model with default parameters. ExtraTrees is a tree-structure method based on plenty of binary decision trees (Geurts P et al., 2006), while RandomForest is composed of multiple unrelated decision trees (Breiman L, 2001), both of which have two parameters of Gini index and information entropy. The last two models with different parameters, NeuralNetFastAI and NeuralNetTorch, are neural network models implemented in two frameworks, PyTorch and FastAI, respectively. By training the above 13 base machine learning models, the results are weighted to merge the final output model WeightedEnsemble.

2.4. Model validation

The comprehensive performance of the models, including efficiency and applicability, needs to be assessed quantitatively using certain metrics. In this study, four metrics were selected to validate and compare the performance of the models: The receiver operating characteristic (ROC) curve, precision, recall, and accuracy. The ROC curve is a common visualization method, which is a line drawn by connecting points with true positive rate (TPR) as the vertical axis and false positive rate (FPR) as the horizontal axis. After the quantitative evaluation of model performance by measuring the AUC value (Fawcett T, 2006; Nhu VH et al., 2020), higher values of the above four metrics represent better model performance, and they can be calculated using the following equations:

$$Accuracy = \frac{TP+TN}{TP+TN+FP+FN} \tag{2}$$

$$\mathrm{Precision} = \frac{TP}{TP+FP} \tag{3}$$

$$Recall = \frac{TP}{TP+FN} \tag{4}$$

$$TPR = \frac{TP}{TP+FN} \tag{5}$$

$$FPR = \frac{FP}{TN+FP} \tag{6}$$

where *TP* denotes true positive, indicating that the landslide sample is correctly labeled as "landslide" by the model, *FP* represents false positive, indicating that the non-landslide sample is labeled as "landslide" by the model, *TN* is true negative, indicating that the non-landslide sample is correctly labeled as "non-landslide" by the model, and *FN* is "false false negative", indicating that the landslide sample is labeled as "non-landslide" by the model.

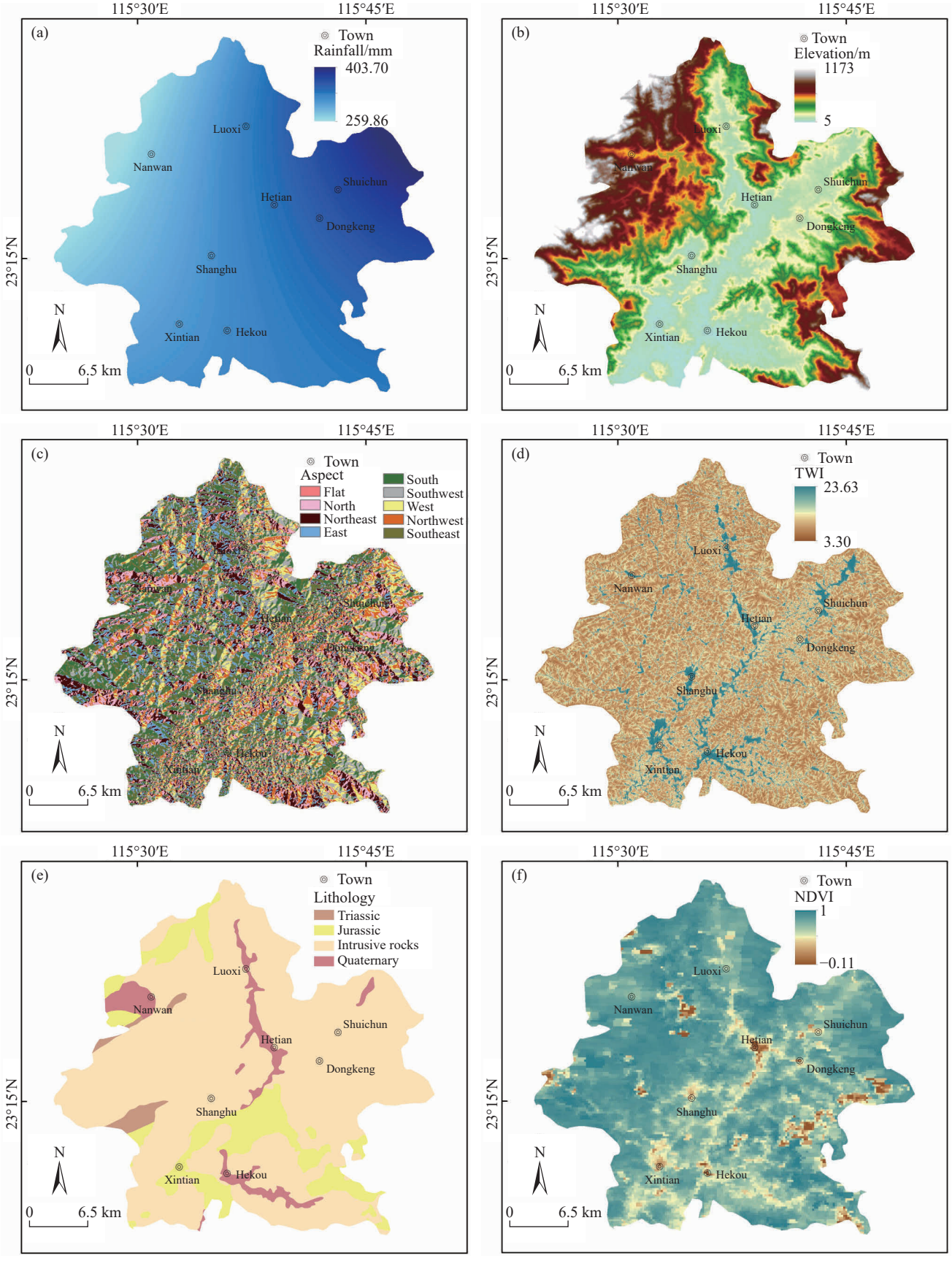

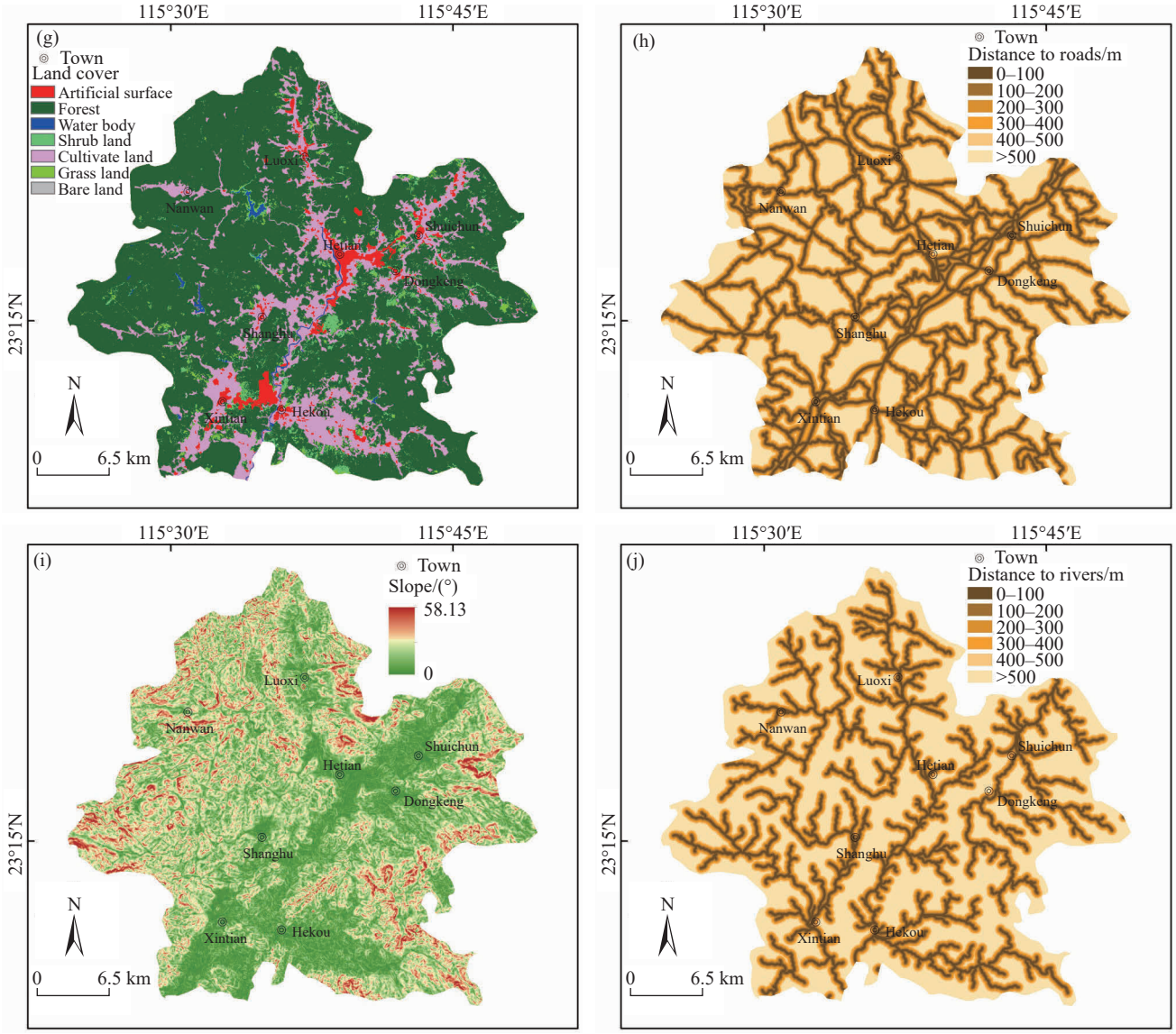

Fig. 5. Landslide causative factors. a–rainfall; b–elevation; c–aspect; d–TWI; e–lithology; f–NDVI; g–land cover; h–distance to roads; i–slope; j–distance to rivers.

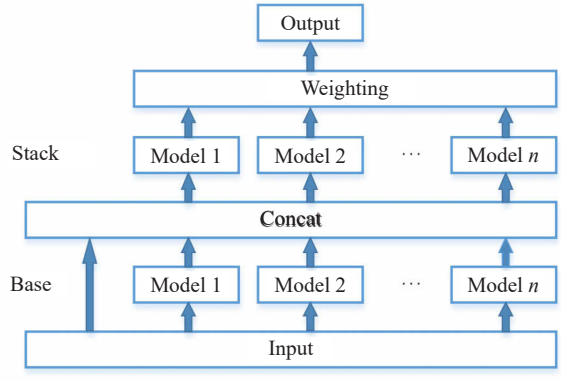

Fig. 6. AutoGluon's multi-layer stacking strategy. Structure of two stacking layers and n types of base learners (after Erickson N et al., 2020).

3. Results and analysis

3.1. Selection of impact factors

The results of the correlation matrix are shown in Fig. 7. A number of studies have shown that when the absolute value of the correlation coefficient is greater than 0.7, a high collinearity exists between variables. On the contrary, it means that all variables can meet the requirements of the correlation test (Dormann CF et al., 2013; Tien Bui D et al., 2016; Kornejady A et al., 2017; Yao JY et al., 2020). Therefore, this article selects 0.7 as the correlation coefficient threshold based on expert experience. Overall, the correlation coefficient ranges from −0.47 to 0.4. The absolute value of the correlation coefficient between slope and TWI is the largest (0.47), which is not higher than 0.7, demonstrating that 10 influencing factors all passed the correlation test and are valid for this landslide hazard assessment.

3.2. Model performance

Table 2 shows the performance of the 14 models in training and test. During the training process, the time used for preprocessing and model training for all models was

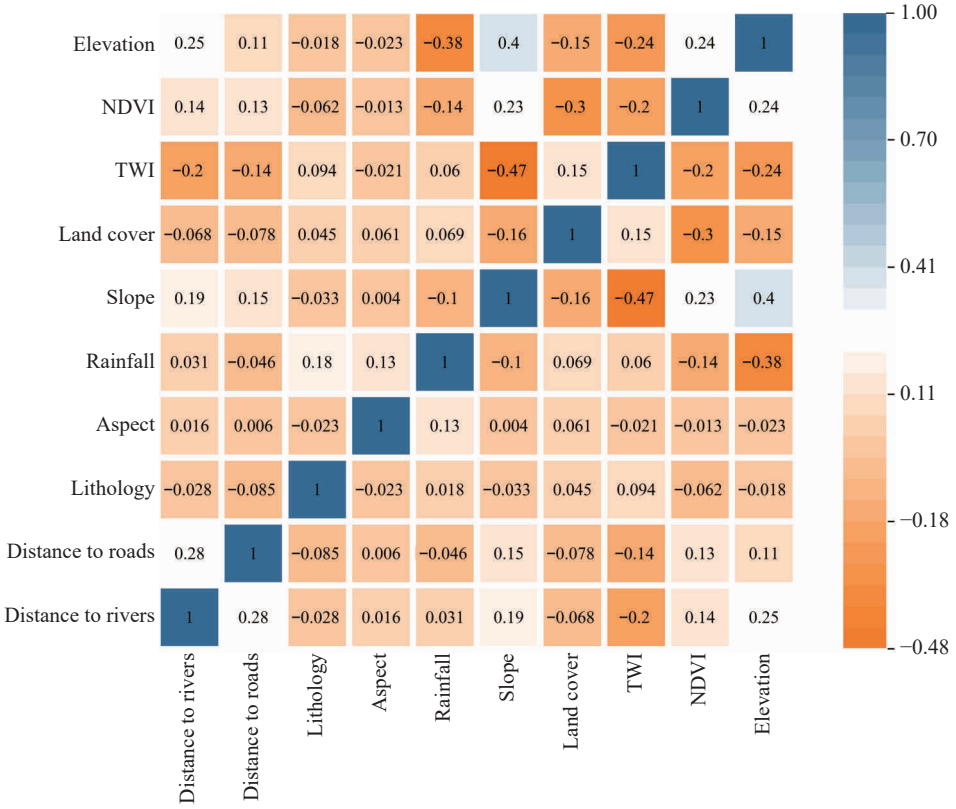

Fig. 7. Output results of the correlation matrix.

Table 2. Training and test performance of all models (Bolded for the WeightedEnsemble model).

Models		Training performance			Testing performance			
		AUC/%	Accuracy/%	Time/s	AUC/%	Precision/%	Recall/%	Accuracy/%
1	KNeighborsDist	98.42	66.8	0.06	78.93	68.80	78.66	72.19
2	KNeighborsUnif	86.10	66.8	13.54	77.17	67.42	77.29	70.71
3	CatBoost	98.67	83.4	9.77	91.37	81.40	86.74	83.87
4	XGBoost	98.76	82.8	1.57	91.13	80.86	85.67	83.12
5	RandomForestEntr	99.48	81.8	2.55	92.02	81.09	86.28	83.49
6	RandomForestGini	99.48	81.0	3.7	91.70	80.65	86.43	83.27
7	ExtraTreesGini	99.57	81.2	1.66	92.11	79.92	89.79	84.01
8	ExtraTreesEntr	99.58	82.2	1.68	92.06	79.46	89.63	83.64
9	LightGBM	97.58	81.6	1.98	90.82	79.30	85.82	82.16
10	LightGBMLarge	99.49	82.8	5.1	92.35	80.98	87.65	83.94
11	LightGBMXT	98.77	82.8	12.47	90.66	78.87	85.36	81.71
12	NeuralNetTorch	90.55	81.8	24.32	87.50	75.40	86.43	79.63
13	NeuralNetFastAI	92.66	81.0	22.52	88.13	75.22	89.33	80.45
14	**WeightedEnsemble**	**99.46**	**84.6**	**1.52**	**92.36**	**82.18**	**87.20**	**84.54**

102.44 s. The last ensemble model, WeightedEnsemble, took 1.52 s. Meanwhile, the WeightedEnsemble model achieved the highest accuracy of 84.6%. Among the 13 basic models, the CatBoost model showed the best accuracy of 83.4%. Additionally, according to the model success rate ROC curve (Fig. 8a), it can be noticed that the AUC values of all models were greater than 85%, indicating that the models were well-fitted and had high accuracy. In the test performance, Table 2 and the model prediction rate ROC curve (Fig. 8b) revealed that the AUC value, precision, recall, and accuracy of WeightedEnsemble model were 92.36%, 82.18%, 87.20%, and 84.54%, respectively. The AUC value, precision, and accuracy were the highest among all the models, and the recall was only 2.88% lower than the highest value. The results demonstrate the reliability of the model for subsequent landslide hazard assessment. In summary, the WeightedEnsemble model had the best overall performance in AUC value, precision, recall, and accuracy, indicating its excellent predictive capability.

3.3. Landslide hazard assessment

Due to the outstanding performance, the WeightedEnsemble model was selected for landslide hazard

mapping in Luhe County. The Jenks natural breaks method was used to classify the assessment results, and five categories were obtained: very low, low, medium, high, and very high (Fig. 9). It is obvious that the high and very high hazard areas are continuously adjacent in the northern, central, and southwestern regions, mainly distributed in the lower-elevation regions of the study area. At the same time, the landslide locations align well with the high and very high hazard classes. The very low hazard class is distributed in the southeastern, northwestern, and western of the relatively high elevation, as well as the intermediate plain areas.

For a more objective analysis, the statistics of classification areas and the number of landslides within different classes are presented. Fig. 10 exhibits the statistics of landslide hazard classification area, landslide density, and the percentage of landslide number. It should be noted that when counting the number of landslides, there was a landslide that did not fall into the hazard assessment results. The reason for this phenomenon is that the hazard assessment results are in raster format, which inevitably does not fit perfectly with the vector boundary of the study area. Hence, there is a landslide within the study area but outside the hazard assessment results. However, compared with the total landslide number (2241), one landslide does not significantly affect the overall statistical results. Therefore, when calculating the percentage of landslides, this landslide was excluded, and only 2240

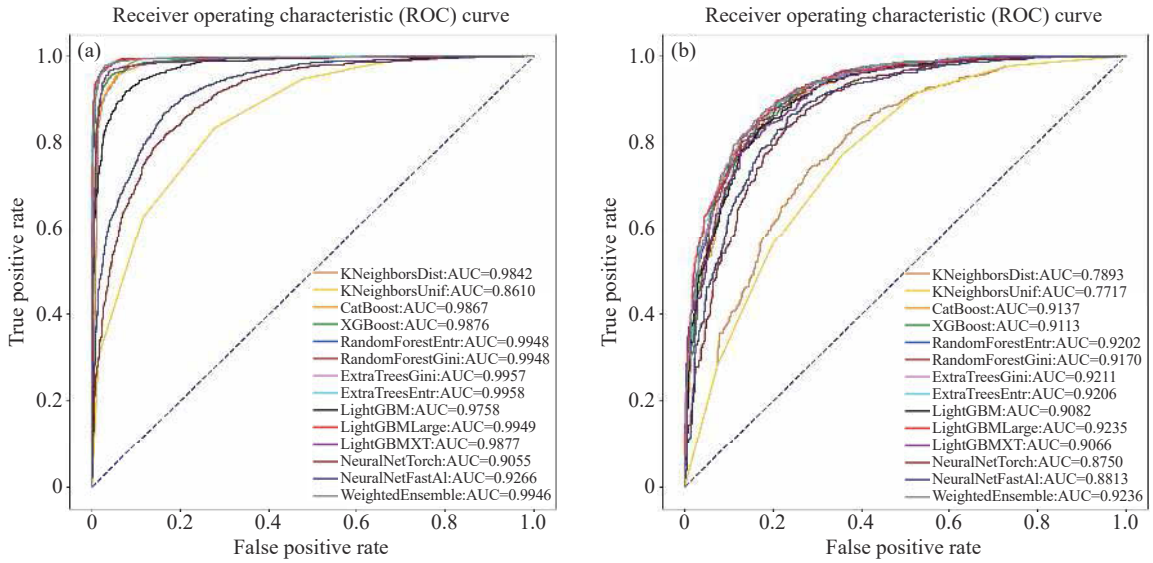

Fig. 8. ROC curves and AUC values of all models. a–success rate; b–prediction rate.

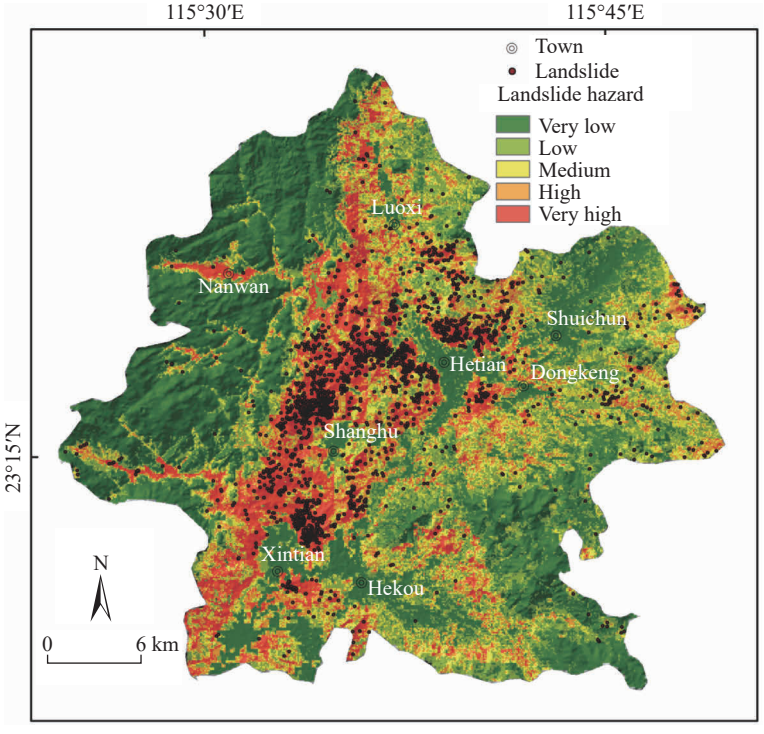

Fig. 9. Landslide hazard map produced by the WeightedEnsemble model.

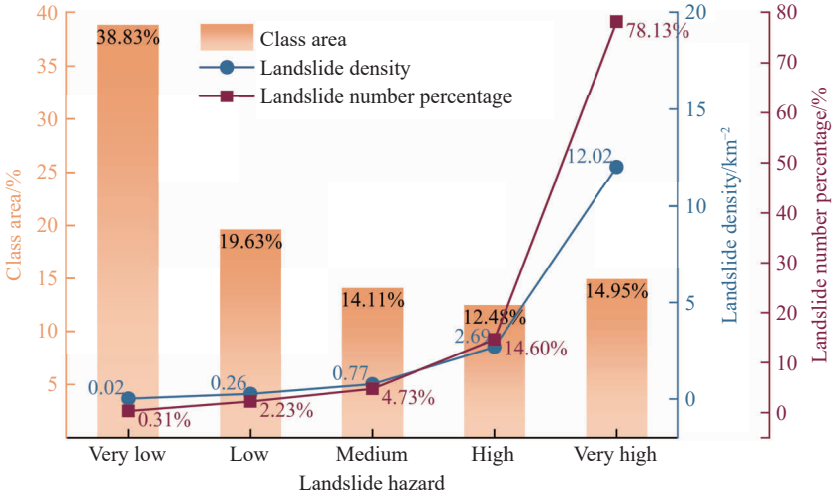

Fig. 10. Percentage of area, landslide density and number percentage by hazard classes.

landslides were counted. The statistics show that 14.95% of the area is in very high hazard class, with a landslide density of 12.02/km^2, and a total of 78.13% (1750 landslides) of the landslides fall into it. The high hazard class accounts for 12.48% of the area, with a landslide density of 2.69/km^2 and contains 14.60% (327 landslides) of the total landslides. The remaining three classes (i.e. very low, low, and medium hazard classes) account for 38.83%, 19.63%, and 14.11% of the area, respectively. Overall, there is a decreasing trend from very low to high hazard class, and the area of very high hazard class is 2.47% more than high hazard class. Among the hazard classes that need attention (high and very high), 92.72% of the landslides fall in 27.43% of the area, which not only illustrates the reliability of the model, but also indicates the seriously high landslide risk in the Luhe County.

4. Discussion

It is well acknowledged that the occurrence of landslides are associated with numerous factors, and factor weights can demonstrate the contribution of factors to landslide occurrence. To a certain extent, the results of factor weight analysis can be regarded as a reflection of the relationship between factors and landslides. In the landslide hazard assessment of Luhe County, 10 influencing factors were selected for weight analysis based on the availability and accessibility of data. Substantial studies have indicated that rainfall is a crucial triggering factor for landslides (Zhang TL et al., 2020; Bai HL et al., 2021; Zhang S et al., 2021; Feng WK et al., 2022; Shao XY et al., 2023; Yu B et al., 2023). Heavy rainfall events can result in abundant rainwater infiltrating into the rock-soil mass, which weakens the shear strength between the rock-soil masses. As a result, the softening of potential sliding surfaces occurs, providing favorable conditions for landslide occurrence. The results of the factor weights (Fig. 11) showed that rainfall plays the most significant role in landslide occurrence, thus possessing the largest weight (0.1508) among all factors. Among the non-triggering factors, elevation has the greatest weight (0.1233). Figs. 1–3 show that landslides are not predominantly distributed in the relatively high-elevation mountainous areas in the northwest of the study area, but rather are found in the lower mountainous areas that are adjacent to areas with human activities. Such a phenomenon is consistent with the pattern of rainfall-induced landslides in the southeastern coastal regions of China (e.g. Yu B et al., 2023; Ma SY et al., 2022; Liang X et al., 2022). These studies suggested that anthropogenic factors such as engineering activities and land-use changes may be responsible for the local hazards. Indeed, different elevations can have varying effects on slope stability, and elevation is pervasively considered as a typical factor in landslide assessments (Xu C et al., 2013; Wu H and Song T, 2018; Wang HP et al., 2023).

It is worth noting that rainfall, as the factor with the highest weight, is higher in the east than in the west in the study area (Fig. 5a). This differs somewhat from the fact that landslides primarily occur in the central part of the study area. If only the spatial distribution of rainfall and landslides is considered, the difference indeed exists. However, landslides are associated with the combined effect of multiple factors, and are also influenced by many other conditions in addition to rainfall. Therefore, the spatial distribution of landslides does not strictly correspond to the rainfall. Furthermore, occasionality may exist in such a small local area, and rainfall data may not completely reflect the actual situation. For instance, there is no national rainfall station in Luhe County, and thus the rainfall data are collected based on thestation adjacent to Luhe County. The interpolated data derived from station data represents an average characteristic, which may not accurately reflect rainfall differences in a small local area (Herrera S et al., 2019). However, in landslide hazard analysis, many scholars have obtained satisfactory results using interpolated rainfall products (Huangfu WC et al., 2021; Cui YL et al., 2022; Ma SY et al., 2023c). Overall, the data in this study meet the requirements and are valuable for landslide hazard analysis.

Inspired by the successful application of single machine learning models in landslide hazard assessment, researchers

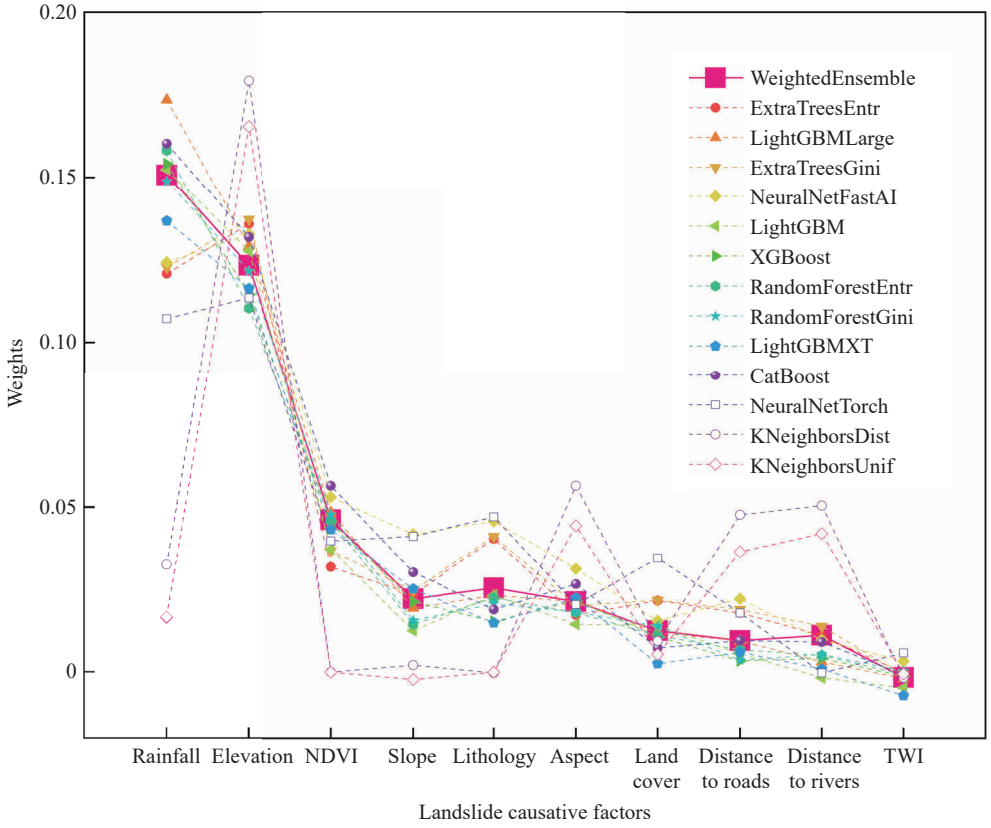

Fig. 11. Results of factor weights for all models.

have attempted to apply ensemble learning in landslide hazard analysis and compare it with other machine learning models. Numerous studies have demonstrated that ensemble learning models perform better than single machine learning models (Zhang YH et al., 2019; Zhou XT et al., 2021; Ling X et al., 2022). Although machine learning models generally exhibit superior performance in landslide hazard assessment, there are still some uncertainties in black-box models. For instance, the interpretability of the model is still a challenging issue (Reichenbach P et al., 2018). While machine learning models can improve the accuracy of landslide hazard analysis, it is difficult to provide interpretable insights into the relationship between landslides and condition factors, and understanding how these algorithms make decisions can be a challenging endeavor. In recent years, some scholars have begun to explore the application of interpretability techniques including SHAP (Al-Najjar HAH et al., 2022; Zhou XZ et al., 2022), LIME (Sun DL et al., 2022), and PDP (Sun DL et al., 2022) in landslide hazard analysis. These methods aim to elucidate the dominant factors influencing prediction outcomes, assisting decision-makers in comprehending the intrinsic mechanisms of the model.

5. Conclusions

In this study, a visual interpretation of satellite images was conducted to identify rainfall-induced landslides in Luhe County in Guangdong Province, China. During the landslide modeling process, 10 influencing factors were selected. The WeightedEnsemble model was weighted and assembled by 13 basic machine learning models, and was subsequently used for landslide hazard mapping. Major findings and conclusions of this study include the following:

(i) Based on the high-resolution satellite images, totally 2241 rainfall-induced landslides were identified by visual interpretation. These landslides predominantly occurred in Hetian and Shanghu town, and were mostly clustered shallow and narrow landslides. The smallest landslide area in the study area is 126 m^2, and the largest landslide area is 19761 m^2. Additionally, the maximum landslide density is 54.03/km^2. Factor weight analysis revealed that rainfall, as a triggering factor, played the most significant role in influencing landslide occurrence, followed by elevation. All machine learning models performed well, but the WeightedEnsemble model performed the best in the training set with an accuracy of 84.6%. In the test performance, the WeightedEnsemble model achieved an AUC value of 92.36%.

(ii) Based on the Jenks natural breaks method, the hazard assessment results were classified into five categories: Very low, low, medium, high, and very high. The results show that the very high and high hazard zones are predominantly located in the northern, central, and southwestern parts of the Luhe County. The very low hazard zone is distributed in the southeastern, northwestern, and some western areas of the study area. Meanwhile, the area of very high and high hazard classes account for 14.95% and 12.48% of the total areas, respectively, and the corresponding landslide densities are 12.02/km^2 and 2.69/km^2, respectively. These findings emphasize that the future landslide hazard risk in Luhe

County should not be overlooked. In summary, we conducted a rainfall-induced landslides hazard assessment in Luhe County using the AutoGluon and obtained a reliable landslide hazard map in this study. This study not only provides technical support for landslide risk management in Luhe County but also broadens the application range of ensemble models in landslide hazards.

CRediT authorship contribution statement

Tao Li, Chen-chen Xie, Chong Xu and Wen-wen Qi conceived of the presented idea. Chen-chen Xie and Lei Li carried out the experiment. Tao Li and Yuan-dong Huang wrote the manuscript in consultation. Chong Xu provided the necessary data. All authors discussed the results and contributed to the final manuscript.

Declaration of competing interest

The authors declare no conflicts of interest.

Acknowledgments

This study was supported by the State Administration of Science, Technology and Industry for National Defence, PRC (KJSP2020020303) and the National Institute of Natural Hazards, Ministry of Emergency Management of China (ZDJ2021-12).

References

Abella EAC, Van Westen CJ. 2008. Qualitative landslide susceptibility assessment by multicriteria analysis: A case study from San Antonio del Sur, Guantánamo, Cuba. Geomorphology, 94(3–4), 453–466. doi: 10.1016/j.geomorph.2006.10.038.

Abuzied SM, Alrefaee HA. 2019. Spatial prediction of landslide-susceptible zones in El-Qaá area, Egypt, using an integrated approach based on GIS statistical analysis. Bulletin of Engineering Geology and the Environment, 78, 2169–2195. doi: 10.1007/s10064-018-1302-x.

Al-Najjar HAH, Pradhan B, Beydoun G, Sarkar R, Park HJ, Alamri A. 2022. A novel method using explainable artificial intelligence (XAI)-based Shapley Additive Explanations for spatial landslide prediction using time-series SAR dataset. Gondwana Research, 123(2023), 107–124. doi: 10.1016/j.gr.2022.08.004.

Ali MZ, Chu HJ, Chen YC, Ullah S. 2021. Machine learning in earthquake-and typhoon-triggered landslide susceptibility mapping and critical factor identification. Environmental Earth Sciences, 80, 233. doi: 10.1007/s12665-021-09510-z.

Bai HL, Feng WK, Yi XY, Fang HY, Wu YY, Deng PC, Dai HC, Hu R. 2021. Group-occurring landslides and debris flows caused by the continuous heavy rainfall in June 2019 in Mibei Village, Longchuan County, Guangdong Province, China. Natural Hazards, 108(3), 3181–3201. doi: 10.1007/s11069-021-04819-1.

Baum RL, Godt JW, Savage WZ. 2010. Estimating the timing and location of shallow rainfall-induced landslides using a model for transient, unsaturated infiltration. Journal of Geophysical Research: Earth Surface, 115(F3), F03013. doi: 10.1029/2009JF001321.

Breiman L. 2001. Random forests. Machine Learning, 45, 5–32. doi: 10.1023/A:1010933404324.

Chen W, Zhang S, Li RW, Shahabi H. 2018. Performance evaluation of the GIS-based data mining techniques of best-first decision tree, random forest, and naïve Bayes tree for landslide susceptibility modeling. Science of the Total Environment, 644, 1006–1018. doi: 10.1016/j.scitotenv.2018.06.389.

Cui YL, Bao PP, Xu C, Ma SY, Zheng J, Fu G. 2021. Landslides triggered by the 6 September 2018 Mw6.6 Hokkaido, Japan: An updated inventory and retrospective hazard assessment. Earth Science Informatics, 14, 247–258. doi: 10.1007/s12145-020-00544-8.

Cui YL, Jin JL, Huang QB, Yuan K, Xu C. 2022. A data-driven model for spatial shallow landslide probability of occurrence due to a typhoon in Ningguo City, Anhui Province, China. Forests, 13(5), 732. doi: 10.3390/f13050732.

Cui YL, Yang WH, Xu C, Wu S. 2023. Distribution of ancient landslides and landslide hazard assessment in the Western Himalayan Syntaxis area. Frontiers in Earth Science, 11, 1135018. doi: 10.3389/feart.2023.1135018.

Dai FC, Lee CF. 2002. Landslide characteristics and slope instability modeling using GIS, Lantau Island, Hong Kong. Geomorphology, 42(3-4), 213–228. doi: 10.1016/S0169-555X(01)00087-3.

Dormann CF, Elith J, Bacher S, Buchmann C, Carl G, Carré G, Marquéz JRG, Gruber B, Lafourcade B, Leitão PJ. 2013. Collinearity: A review of methods to deal with it and a simulation study evaluating their performance. Ecography, 36(1), 27–46. doi: 10.1111/j.1600-0587.2012.07348.x.

Dou J, Yunus AP, Bui DT, Merghadi A, Sahana M, Zhu ZF, Chen CW, Khosravi K, Yang Y, Pham BT. 2019. Assessment of advanced random forest and decision tree algorithms for modeling rainfall-induced landslide susceptibility in the Izu-Oshima Volcanic Island, Japan. Science of the Total Environment, 662, 332–346. doi: 10.1016/j.scitotenv.2019.01.221.

Erickson N, Mueller J, Shirkov A, Zhang H, Larroy P, Li M, Smola A. 2020. Autogluon-tabular: Robust and accurate automl for structured data. arXiv preprint arXiv: 2003.06505,doi: 10.48550/arXiv.2003.06505.

Fan W, Wei XS, Cao YB, Zheng B. 2017. Landslide susceptibility assessment using the certainty factor and analytic hierarchy process. Journal of Mountain Science, 14(5), 906–925. doi: 10.1007/s11629-016-4068-2.

Fawcett T. 2006. An introduction to ROC analysis. Pattern Recognition Letters, 27(8), 861–874. doi: 10.1016/j.patrec.2005.10.010.

Fell R, Corominas J, Bonnard C, Cascini L, Leroi E, Savage WZ. 2008. Guidelines for landslide susceptibility, hazard and risk zoning for land use planning. Engineering Geology, 102(3-4), 99–111. doi: 10.1016/j.enggeo.2008.03.014.

Feng WK, Bai HL, Lan B, Wu YY, Wu ZT, Yan LZ, Ma XJ. 2022. Spatial–temporal distribution and failure mechanism of group-occurring landslides in Mibei Village, Longchuan County, Guangdong, China. Landslides, 19(8), 1957–1970. doi: 10.1007/s10346-022-01904-9.

Geurts P, Ernst D, Wehenkel L. 2006. Extremely randomized trees. Machine Learning, 63, 3–42. doi: 10.1007/s10994-006-6226-1.

Guo ZZ, Tian BX, He J, Xu C, Zeng TR, Zhu YH. 2023. Hazard assessment for regional typhoon-triggered landslides by using physically-based model–A case study from southeastern China. Georisk: Assessment and Management of Risk for Engineered Systems and Geohazards, 17(4), 740–754. doi: 10.1080/17499518.2023.2188465.

Haque U, Da Silva PF, Devoli G, Pilz J, Zhao B, Khaloua A, Wilopo W, Andersen P, Lu P, Lee J. 2019. The human cost of global warming: Deadly landslides and their triggers (1995–2014). Science of the Total Environment, 682, 673–684. doi: 10.1016/j.scitotenv.2019.03.415.

Herrera S, Kotlarski S, Soares PMM, Cardoso RM, Jaczewski A, Gutiérrez JM, Maraun D. 2019. Uncertainty in gridded precipitation

products: Influence of station density, interpolation method and grid resolution. International Journal of Climatology, 39(9), 3717–3729. doi: 10.1002/joc.5878.

Hong HY, Xu C, Bui DT. 2015. Landslide susceptibility assessment at the Xiushui area (China) using frequency ratio model. Procedia Earth and Planetary Science, 15, 513–517. doi: 10.1016/j.proeps.2015.08.065.

Huang YD, Li L, Xu C, Cheng J, Xu XW, Zheng TY, Zhang XJ. 2022. Spatiotemporal distribution patterns of deadly geohazard events in China, 2013–2019. Natural Hazards Research, 2(4), 316–324. doi: 10.1016/j.nhres.2022.10.003.

Huangfu WC, Wu WC, Zhou XT, Lin ZY, Zhang GL, Chen RX, Song Y, Lang T, Qin YZ, Ou PH. 2021. Landslide geo-hazard risk mapping using logistic regression modeling in Guixi, Jiangxi, China. Sustainability, 13(9), 4830. doi: 10.3390/su13094830.

Hungr O, Leroueil S, Picarelli L. 2014. The Varnes classification of landslide types, an update. Landslides, 11, 167–194. doi: 10.1007/s10346-013-0436-y.

Ke GL, Meng Q, Finley T, Wang TF, Chen W, Ma WD, Ye QW, Liu TY. 2017. Lightgbm: A highly efficient gradient boosting decision tree. In: Proceedings of the 31st International Conference on Neural Information Processing Systems, 3149–3157.

Ko Ko C, Flentje P, Chowdhury R. 2004. Landslides qualitative hazard and risk assessment method and its reliability. Bulletin of Engineering Geology and the Environment, 63, 149–165. doi: 10.1007/s10064-004-0231-z.

Kornejady A, Ownegh M, Bahremand A. 2017. Landslide susceptibility assessment using maximum entropy model with two different data sampling methods. Catena, 152, 144–162. doi: 10.1016/j.catena.2017.01.010.

Li XS, Li QH, Hu YJ, Chen QS, Peng J, Xie YL, Wang JW. 2022. Study on three-dimensional dynamic stability of open-pit high slope under blasting vibration. Lithosphere, (Special 4), 6426550. doi: 10.2113/2022/6426550.

Liang X, Segoni S, Yin KL, Du J, Chai B, Tofani V, Casagli N. 2022. Characteristics of landslides and debris flows triggered by extreme rainfall in Daoshi Town during the 2019 Typhoon Lekima, Zhejiang Province, China. Landslides, 19(7), 1735–1749. doi: 10.1007/s10346-022-01889-5.

Ling X, Zhu YQ, Ming DP, Chen YY, Zhang L, Du TY. 2022. Feature engineering of geohazard susceptibility analysis based on the random forest algorithm: Taking Tianshui City, Gansu Province, as an example. Remote Sensing, 14(22), 5658. doi: 10.3390/rs14225658.

Ma SY, Shao XY, Xu C. 2022. Characterizing the distribution pattern and a physically based susceptibility assessment of shallow landslides triggered by the 2019 heavy rainfall event in Longchuan County, Guangdong Province, China. Remote Sensing, 14(17), 4257. doi: 10.3390/rs14174257.

Ma SY, Shao XY, Xu C. 2023a. Estimating the quality of the most popular machine learning algorithms for landslide susceptibility mapping in 2018 Mw7. 5 Palu earthquake. Remote Sensing, 15(19), 4733. doi: 10.3390/rs15194733.

Ma SY, Shao XY, Xu C. 2023b. Physically-based rainfall-induced landslide thresholds for the Tianshui area of Loess Plateau, China by TRIGRS model. Catena, 233, 107499. doi: 10.1016/j.catena.2023.107499.

Ma SY, Shao XY, Xu C. 2023c. Landslides triggered by the 2016 heavy rainfall event in Sanming, Fujian Province: Distribution pattern analysis and spatio-temporal susceptibility assessment. Remote Sensing, 15(11), 2738. doi: 10.3390/rs15112738.

Ma SY, Xu C. 2019. Assessment of co-seismic landslide hazard using the Newmark model and statistical analyses: A case study of the 2013 Lushan, China, Mw6. 6 earthquake. Natural Hazards, 96, 389–412. doi: 10.1007/s11069-018-3548-9.

Montgomery DR, Dietrich WE, Torres R, Anderson SP, Heffner JT, Loague K. 1997. Hydrologic response of a steep, unchanneled valley to natural and applied rainfall. Water Resources Research, 33(1), 91–109. doi: 10.1029/96WR02985.

Nery TD, Vieira BC. 2015. Susceptibility to shallow landslides in a drainage basin in the Serra do Mar, São Paulo, Brazil, predicted using the SINMAP mathematical model. Bulletin of Engineering Geology and the Environment, 74, 369–378. doi: 10.1007/s10064-014-0622-8.

Nhu VH, Hoang ND, Nguyen H, Ngo PTT, Bui TT, Hoa PV, Samui P, Bui DT. 2020. Effectiveness assessment of Keras based deep learning with different robust optimization algorithms for shallow landslide susceptibility mapping at tropical area. Catena, 188, 104458. doi: 10.1016/j.catena.2020.104458.

Panchal S, Shrivastava AK. 2022. Landslide hazard assessment using analytic hierarchy process (AHP): A case study of National Highway 5 in India. Ain Shams Engineering Journal, 13(3), 101626. doi: 10.1016/j.asej.2021.10.021.

Parmanto B, Munro PW, Doyle HR. 1996. Reducing variance of committee prediction with resampling techniques. Connection Science, 8(3-4), 405–426. doi: 10.1080/095400996116848.

Qi WW, Xu C, Xu XW. 2021. AutoGluon: A revolutionary framework for landslide hazard analysis. Natural Hazards Research, 1(3), 103–108. doi: 10.1016/j.nhres.2021.07.002.

Reichenbach P, Rossi M, Malamud BD, Mihir M, Guzzetti F. 2018. A review of statistically-based landslide susceptibility models. Earth-Science Reviews, 180, 60–91. doi: 10.1016/j.earscirev.2018.03.001.

Sahin EK. 2022. Comparative analysis of gradient boosting algorithms for landslide susceptibility mapping. Geocarto International, 37(9), 2441–2465. doi: 10.1080/10106049.2020.1831623.

Shao XY, Ma SY, Xu C, Xu YR. 2023. Insight into the characteristics and triggers of loess landslides during the 2013 heavy rainfall event in the Tianshui Area, China. Remote Sensing, 15(17), 4304. doi: 10.3390/rs15174304.

Singh K, Kumar V. 2018. Hazard assessment of landslide disaster using information value method and analytical hierarchy process in highly tectonic Chamba region in bosom of Himalaya. Journal of Mountain Science, 15(4), 808–824. doi: 10.1007/s11629-017-4634-2.

Sun DL, Gu QY, Wen HJ, Xu JH, Zhang YL, Shi SX, Xue MM, Zhou XZ. 2022. Assessment of landslide susceptibility along mountain highways based on different machine learning algorithms and mapping units by hybrid factors screening and sample optimization. Gondwana Research, 123(2023), 89–106. doi: 10.1016/j.gr.2022.07.013.

Tien Bui D, Tuan TA, Klempe H, Pradhan B, Revhaug I. 2016. Spatial prediction models for shallow landslide hazards: A comparative assessment of the efficacy of support vector machines, artificial neural networks, kernel logistic regression, and logistic model tree. Landslides, 13, 361–378. doi: 10.1007/s10346-015-0557-6.

Tsangaratos P, Ilia I. 2016. Landslide susceptibility mapping using a modified decision tree classifier in the Xanthi Perfection, Greece. Landslides, 13, 305–320. doi: 10.1007/s10346-015-0565-6.

Van Westen CJ, Van Asch TWJ, Soeters R. 2006. Landslide hazard and risk zonation—why is it still so difficult? Bulletin of Engineering Geology and the Environment, 65, 167–184. doi: 10.1007/s10064-005-0023-0.

Wang HP, Wang XD, Zhang CB, Wang C, Li SY. 2023. Analysis on the susceptibility of environmental geological disasters considering regional sustainable development. Environmental Science and Pollution Research, 30(4), 9749–9762. doi: 10.1007/s11356-022-22778-3.

Wang P, Bai XY, Wu XQ, Yu HJ, Hao YR, Hu BX. 2018. GIS-based random forest weight for rainfall-induced landslide susceptibility assessment at a humid region in Southern China. Water, 10(8), 1019.

doi: 10.3390/w10081019.

Wen BY, Xu C, He XL, Ma SY, Shao XY, Li K, Zhang ZJ, Li ZF. 2020. Hazard assessment of co-seismic landslides based on information value method: A case in 2018 Mw6. 6 Hokkaido earthquake, Japan. Earthquake Research in China, 34(1), 64–80. doi: 10.19743/j.cnki.0891-4176.

Wu H, Song T. 2018. An evaluation of landslide susceptibility using probability statistic modeling and GIS's spatial clustering analysis. Human and Ecological Risk Assessment: An International Journal, 24(7), 1952–1968. doi: 10.1080/10807039.2018.1435253.

Xu C, Xu XW, Dai FC, Wu ZD, He HL, Shi F, Wu XY, Xu SN. 2013. Application of an incomplete landslide inventory, logistic regression model and its validation for landslide susceptibility mapping related to the May 12, 2008 Wenchuan earthquake of China. Natural Hazards, 68, 883–900. doi: 10.1007/s11069-013-0661-7.

Xu C, Xu XW, Yao X, Dai FC. 2014. Three (nearly) complete inventories of landslides triggered by the May 12, 2008 Wenchuan Mw7. 9 earthquake of China and their spatial distribution statistical analysis. Landslides, 11, 441–461. doi: 10.1007/s10346-013-0404-6.

Yao JY, Qin SW, Qiao SS, Che WC, Chen Y, Su G, Miao Q. 2020. Assessment of landslide susceptibility combining deep learning with semi-supervised learning in Jiaohe County, Jilin Province, China. Applied Sciences, 10(16), 5640. doi: 10.3390/app10165640.

Yu B, Chen WH, Feng WK, Liu K, Ye LZ. 2023. A case study of shallow landslides triggered by rainfall in Sanming, Fujian Province, China. Environmental Earth Sciences, 82(18), 426. doi: 10.1007/s12665-023-11118-4.

Zhang S, Li C, Peng JY, Peng DL, Xu Q, Zhang Q, Bate B. 2021. GIS-based soil planar slide susceptibility mapping using logistic regression and neural networks: A typical red mudstone area in southwest China. Geomatics, Natural Hazards and Risk, 12(1), 852–879. doi: 10.1080/19475705.2021.1896584.

Zhang TL, Zhou AG, Sun Q, Wang HS, Wu JB, Liu ZH. 2020. Hydrological response characteristics of landslides under typhoon-triggered rainstorm conditions. China Geology, 3(3), 455–461. doi: 10.31035/cg2020028.

Zhang TY, Quevedo RP, Wang HY, Fu Q, Luo D, Wang T, de Oliveira GG, Guasselli LA, Renno CD. 2022. Improved tree-based machine learning algorithms combining with bagging strategy for landslide susceptibility modeling. Arabian Journal of Geosciences, 15(2), 183. doi: 10.1007/s12517-022-09488-3.

Zhang WG, He YW, Wang LQ, Liu SL, Meng XY. 2023. Landslide susceptibility mapping using random forest and extreme gradient boosting: A case study of Fengjie, Chongqing. Geological Journal, 58(6), 2372–2387. doi: 10.1002/gj.4683.

Zhang WG, Liu SL, Wang LQ, Samui P, Chwała M, He YW. 2022. Landslide susceptibility research combining qualitative analysis and quantitative evaluation: A case study of Yunyang County in Chongqing, China. Forests, 13(7), 1055. doi: 10.3390/f13071055.

Zhang YH, Ge TT, Tian W, Liou YA. 2019. Debris flow susceptibility mapping using machine-learning techniques in Shigatse area, China. Remote Sensing, 11(23), 2801. doi: 10.3390/rs11232801.

Zhou XT, Wu WC, Qin YZ, Fu X. 2021. Geoinformation-based landslide susceptibility mapping in subtropical area. Scientific Reports, 11(1), 24325. doi: 10.1038/s41598-021-03743-5.

Zhou XZ, Wen HJ, Li ZW, Zhang H, Zhang WG. 2022. An interpretable model for the susceptibility of rainfall-induced shallow landslides based on SHAP and XGBoost. Geocarto International, 37(26), 13419–13450. doi: 10.1080/10106049.2022.2076928.